

The Possibility of Forming Propargyl Alcohol in the Interstellar Medium

Prasanta Gorai¹, Ankan Das^{1*}, Liton Majumdar^{2,1}, Sandip Kumar Chakrabarti^{3,1}, Bhalamurugan Sivaraman⁴, Eric Herbst⁵

¹Indian Centre for Space Physics, Chalantika 43, Garia Station Rd., Kolkata, 700084, India.

²Laboratoire d'astrophysique de Bordeaux, Univ. Bordeaux, CNRS, B18N, alle Geoffroy Saint-Hilaire, 33615 Pessac, France.

³S. N. Bose National Centre for Basic Sciences, Salt Lake, Kolkata, 700098, India.

⁴Atomic Molecular and Optical Physics Division, Physical Research Laboratory, Ahmedabad, 380009, India.

⁵Departments of Chemistry and Astronomy, University of Virginia, Charlottesville, VA 22904, USA.

Abstract

Propargyl alcohol ($\text{HC}_2\text{CH}_2\text{OH}$, PA) has yet to be observed in the interstellar medium (ISM) although one of its stable isomers, propenal (CH_2CHCHO), has already been detected in Sagittarius B2(N) with the 100-meter Green Bank Telescope in the frequency range 18 – 26 GHz. In this paper, we investigate the formation of propargyl alcohol along with one of its deuterated isotopomers, $\text{HC}_2\text{CH}_2\text{OD}$ (OD-PA), in a dense molecular cloud. Various pathways for the formation of PA in the gas and on ice mantles surrounding dust particles are discussed. We use a large gas-grain chemical network to study the chemical evolution of PA and its deuterated isotopomer. Our results suggest that gaseous $\text{HC}_2\text{CH}_2\text{OH}$ can most likely be detected in hot cores or in collections of hot cores such as the star-forming region Sgr B2(N). A simple LTE (Local thermodynamic equilibrium) radiative transfer model is employed to check the possibility of detecting PA and OD-PA in the millimeter-wave regime. In addition, we have carried out quantum chemical calculations to compute the vibrational transition frequencies and intensities of these species in the infrared for perhaps future use in studies with the James Webb Space Telescope (JWST).

Keywords: Astrochemistry, ISM: molecules, ISM: abundances, ISM: evolution, method: numerical

1. Introduction

The discovery of large numbers of interstellar and circumstellar species regularly refreshes our understanding of the physical conditions of the sources of astrochemical interest (Herbst, 2006). Astronomical observations along with laboratory investigations of various meteoritic samples have discovered the presence of numerous organic molecules of biological interest (Cronin & Chang, 1993). It is also believed that the production of such molecules in star- and planet-forming regions of interstellar clouds, which tend to be partially saturated species containing the elements nitrogen and/or oxygen in addition to carbon and hydrogen, should be connected in some manner with the production of terrestrial bio-molecules. Other types of organic molecules are also present in the ISM. There is strong evidence for species astronomers refer to as “carbon chains” in cold and dense interstellar clouds. These carbon chains are unsaturated and linear species, which can be simple hydrocarbons or species with other heavy atoms such as cyanopolynes, which contain a terminal cyano (CN) group. Various infrared (UIR) emission bands in the 3 – 15 μm range have been observed in different astrophysical sources (Allamandola et al., 1985; Tielens & Allamandola, 1987). Laboratory investigations along with theoretical calculations led to the

hypothesis that the carriers of these bands are aromatic in nature, consisting most probably of free molecular polycyclic aromatic hydrocarbons (PAHs), possibly with other heavy atoms such as nitrogen (Salama & Ehrenfreund, 2014; Noble et al., 2015). Other suggestions include surface functional groups on small grains, quenched carbonaceous composites, amorphous carbon, hydrogenated amorphous carbon and condensed phase PAHs (Brenner & Barker, 1992; Jäger et al., 2009). Recently, two fullerenes, C_{60} and C_{70} , have been discovered in infrared emission in post-stellar objects (Cami et al., 2010) while the cation C_{60}^+ has been confirmed in near-infrared absorption in a diffuse cloud (Walker et al., 2015).

In order to understand the synthesis of PAHs, either in interstellar or circumstellar regions, it is essential to understand the formation of the six-member aromatic species, benzene (C_6H_6). So far there are only two experimentally studied pathways that might result in the synthesis of interstellar or circumstellar benzene. The first is the addition of three acetylene (C_2H_2) molecules (Zhou et al., 2010) and the second is the recombination of two propargyl (C_3H_3) radicals (Wilson et al., 2003). The formation of these radicals could occur in a number of ways. Sharath et al. (2014) carried out an experiment to study the thermal decomposition of PA, and found the products to include OH and C_3H_3 , suggesting that PA could be a precursor to benzene formation. In addition, Sivaraman et al. (2015) found that benzene is the major product from PA irradiation,

*Correspondence author: Ankan Das; Electronic mail: ankan.das@gmail.com

and suggested that the dissociation of PA plays a key role in the synthesis of benzene in interstellar icy mantles.

Since PA might play a crucial role in the formation of PAH molecules, it is of interest to explore various aspects of its interstellar chemistry and spectroscopy in detail. Although PA has not been detected unambiguously in the ISM, propenal (CH_2CHCHO), one of its isomers, has been detected (Hollis et al., 2004) towards the star-forming region Sgr B2(N). Requena et al. (2008) estimated the abundance of CH_2CHCHO to be around $0.3\text{--}2.3 \times 10^{-9}$ with respect to the H_2 molecule in the galactic center. Moreover, PA has a well-known rotational spectrum. Depending upon the internal motion of the OH group, PA could possess two stable conformers, named *gauche* and *trans*. However, microwave studies of PA show that the molecule exists only as the *gauche* isomer, in which the hydroxyl H atom lies $\sim 60^\circ$ out of the $\text{H}-\text{C}\equiv\text{C}-\text{C}-\text{O}$ plane (Hirota, 1968). Pearson & Drouin (2005) summarized other rotational studies of PA, extended the experimental work of Hirota (1968) through 600 GHz and obtained rotational and distortional constants for the *gauche* form of PA and its -OD singly deuterated isotopomer. According to their studies, the *gauche* state is split by inversion into two states, separated by 652.4 GHz for normal PA and 213.5 GHz for the -OD isotopomer. Other spectroscopic work on PA and related species has also been undertaken. Nyquist (1971) recorded and assigned Infrared and Raman spectra for PA, and its deuterated isotopomers, while Devendra & Arunan (2013) carried out experiments to determine the structure of the Ar.PA complex and its two deuterated isotopologues. They found PA to have a *gauche* structure, with Ar located in between the -OH and - $\text{C}\equiv\text{C}-\text{H}$ groups. In another study, Devendra & Arunan (2014) carried out experiments for the pure rotational spectra of the PA dimer and its three deuterium isotopologues.

In this paper, we report the use of our interstellar chemical model to explore various pathways for the formation and destruction of PA (*gauche* form), and to estimate the possibility of detecting this molecule in a dense molecular cloud. Since there are some existing laboratory results for the spectrum of the -OD deuterated form of PA and since some observational evidence for deuterium fractionation of large complex species exists (see for instance $\text{DCOOCH}_3/\text{HCOOCH}_3$, Demyk et al. (2010)), we also consider the -OD isotopomer of PA. Various vibrational transitions of PA are computed and compared with the existing experimental results.

The remainder of this paper is organized as follows. In Section 2, we discuss various reaction pathways and their rate coefficients for the formation and destruction of PA and OD-PA. In Section 3.1, modeling details are presented while in Section 3.2 we discuss modeling results. LTE radiative transfer results are presented in Section 4.1, while computed vibrational spectra for PA and OD-PA are discussed in Section 4.2. Finally, in Section 5, we draw our conclusions.

2. Chemical network

2.1. Formation pathways

In Table 1, all formation and destruction pathways of PA utilized are presented with rate coefficients, if applicable, in both the gas and dust phases. The rate coefficients are shown for two temperatures ($T = 10$ K and 100 K) to represent the temperature dependency (if any). The determination of the rate coefficients actually used is discussed in the next few subsections. Most rate coefficients for the case of deuterated PA are not very different, and are not tabulated. Reaction numbers R1-R6 of Table 1 represent various possible pathways for the formation of PA ($\text{HC}_2\text{CH}_2\text{OH}$). Reaction numbers R1-R5 are found to be exothermic in both phases and are included in our network. The reaction exothermicities or endothermicities for all these reactions have been calculated by using the Gaussian 09 (Frisch et al., 2009) program with a B3LYP functional (Becke, 1988; Lee et al., 1988) and basis set 6-311g++(d,p). Note that reaction exothermicities or endothermicities do not differ significantly between the gaseous and ice mantle phases. We calculated the endothermicity/exothermicity (ΔH) of a reaction by taking the difference between the total optimized enthalpy including zero point corrections of the products and reactants. If ΔH is positive, we label the reaction endothermic and if ΔH is negative, we label the reaction exothermic. Another formation reaction, R6, is considered only in the gas phase. The individual formation reactions are discussed in the following paragraphs.

Reaction R1 ($\text{O} + \text{C}_3\text{H}_3$) in the gas phase was studied by Kwon et al. (2006), who carried out an experiment as well as ab initio statistical calculations. They found that the reaction is barrier-less and can produce propynal (HC_2CHO) and H. The conversion of propynal into PA then can occur via two association reactions (R3, R4) with atomic hydrogen. In the gas phase, the process occurs via radiative association, in which emission of a photon stabilizes the intermediate reaction complex. Lee et al. (2006) predicted that the barrier-less addition of $\text{O}(^3\text{P})$ to propargyl radical (C_3H_3) on the lowest doublet potential energy surface could produce several energy-rich intermediates, which undergo subsequent isomerization and decomposition steps to generate various exothermic reaction products. Their statistical calculation also suggests that the primary reaction channel leads to the formation of propynal. Reaction R2, in which the radical CCH and formaldehyde produce propynal + H, was studied by Dong et al. (2005) and by Petrie (1995). Dong et al. (2005) calculated a very small barrier of 2.1 kcal/mol at the highest level of theory, while Petrie (1995) assumed the channel to be barrier-less based on similar reactions. The propynal product can then also be hydrogenated to PA via R3 and R4.

As an alternative to two successive H-atom association reactions involving atomic hydrogen, we checked the reaction of H_2 with propynal (HC_2CHO) to form PA but found it to be highly endothermic. We tried a few other pathways for the formation of PA via single step reactions, sometimes involving a radical. In this effort, we considered the reaction between C_2H_4 and CO, the reaction between propynal and H_2O , and the reaction between the propargyl radical and OH (reaction number R5). The reactions between C_2H_4 and CO and between

Table 1: Formation and destruction pathways of PA and its related species.

Reaction number (type)	Reaction	α	β	γ	Gas phase rate coefficient at $T = 10$ K (100 K)	Ice phase rate coefficient at $T = 10$ K (100K)
Formation pathways						
R1 (NR)	$O(^3P) + C_3H_3 \rightarrow HC_2CHO + H(-252.30^a, -231.11^b)$	2.3×10^{-10}	0.0	0.0	$2.3 \times 10^{-10} (2.3 \times 10^{-10})^x$	$2.83 \times 10^{-7} (2.51 \times 10^4)^y$
R2 (NR)	$C_2H + H_2CO \rightarrow HC_2CHO + H(-109.17^a, -106.307^b)$	1.00×10^{-10}	0.0	0.0	$1.00 \times 10^{-10} (1.00 \times 10^{-10})^x$	$2.84 \times 10^{-17} (3.03 \times 10^3)^y$
R3 (NR)	$HC_2CHO + H \rightarrow HC_2CH_2O(-86.69^a, -86.23^b)$	-	-	-	$0(1.96 \times 10^{-15})^x$	$6.24 \times 10^{-9} (8.94 \times 10^{-3})^y$
R4 (RR)	$HC_2CH_2O + H \rightarrow HC_2CH_2OH(-420.35^a, -421.67^b)$	1.00×10^{-10}	0.0	0.0	$1.00 \times 10^{-10} (1.00 \times 10^{-10})^x$	$1.77 \times 10^{-1} (2.54 \times 10^5)^y$
R5 (RR)	$C_3H_3 + OH \rightarrow HC_2CH_2OH(-301.35^a, -298.97^b)$	1.00×10^{-10}	0.0	0.0	$1.00 \times 10^{-10} (1.00 \times 10^{-10})^x$	$7.86 \times 10^{-29} (2.19 \times 10^2)^y$
R6 (DR)	$HC_2CH_2OH_2^+ + e^- \rightarrow HC_2CH_2OH + H$	2.67×10^{-8}	-0.59	0.0	$2.00 \times 10^{-7} (5.16 \times 10^{-8})^x$	-
Destruction pathways						
R7 (NR)	$HC_2CH_2OH + OH \rightarrow HOC_2HHCHOH$	9.20×10^{-12}	0.0	0.0	$9.20 \times 10^{-12} (9.20 \times 10^{-12})^x$	$3.58 \times 10^{-38} (3.64 \times 10^1)^y$
R8 (NR)	$HC_2CH_2OH + OD \rightarrow HOC_2HHCHOD$	9.20×10^{-12}	0.0	0.0	$9.20 \times 10^{-12} (9.20 \times 10^{-12})^x$	$3.48 \times 10^{-38} (3.54 \times 10^1)^y$
R9 (IN)	$HC_2CH_2OH + C^+ \rightarrow HC_2CH_2O^+ + CH$	2.03×10^{-9}	-0.5	0.0	$1.22 \times 10^{-8} (4.63 \times 10^{-9})^x$	-
R10 (IN)	$HC_2CH_2OH + C^+ \rightarrow C_3H_3^+ + HCO$	2.03×10^{-9}	-0.5	0.0	$1.22 \times 10^{-8} (4.61 \times 10^{-9})^x$	-
R11 (IN)	$HC_2CH_2OH + H_3O^+ \rightarrow HC_2CH_2OH_2^+ + H_2O$	1.70×10^{-9}	-0.5	0.0	$1.02 \times 10^{-8} (3.85 \times 10^{-9})^x$	-
R12 (IN)	$HC_2CH_2OH + HCO^+ \rightarrow HC_2CH_2OH_2^+ + CO$	1.46×10^{-9}	-0.5	0.0	$8.79 \times 10^{-9} (3.32 \times 10^{-9})^x$	-
R13 (IN)	$HC_2CH_2OH + H_3^+ \rightarrow C_3H_3^+ + H_2O + H_2$	3.78×10^{-9}	-0.5	0.0	$2.27 \times 10^{-8} (8.56 \times 10^{-9})^x$	-
R14 (IN)	$HC_2CH_2OH + H_3^+ \rightarrow HC_2CH_2OH_2^+ + H_2$	3.78×10^{-9}	-0.5	0.0	$2.27 \times 10^{-8} (8.56 \times 10^{-9})^x$	-
R15 (IN)	$HC_2CH_2OH + He^+ \rightarrow C_3H_3^+ + He + OH$	3.31×10^{-9}	-0.5	0.0	$1.99 \times 10^{-8} (7.51 \times 10^{-9})^x$	-
R16 (IN)	$HC_2CH_2OH + He^+ \rightarrow C_3H_3 + He + OH^+$	3.31×10^{-9}	-0.5	0.0	$1.99 \times 10^{-8} (7.51 \times 10^{-9})^x$	-
R17 (IN)	$HC_2CH_2OH + CH_3^+ \rightarrow HC_2CH_2O^+ + CH_4$	1.86×10^{-9}	-0.5	0.0	$1.12 \times 10^{-8} (4.21 \times 10^{-9})^x$	-
R18 (IN)	$HC_2CH_2OH + H^+ \rightarrow C_3H_3^+ + H_2O$	6.43×10^{-9}	-0.5	0.0	$3.86 \times 10^{-8} (1.46 \times 10^{-8})^x$	-
R19 (IN)	$HC_2CH_2OH + H^+ \rightarrow HC_2CH_2O^+ + H_2$	6.43×10^{-9}	-0.5	0.0	$3.86 \times 10^{-8} (1.46 \times 10^{-8})^x$	-
R20 (IN)	$HC_2CH_2OH + H^+ \rightarrow HC_2CH_2O^+ + H_2 + H_2$	6.43×10^{-9}	-0.5	0.0	$3.86 \times 10^{-8} (1.46 \times 10^{-8})^x$	-
R21 (IN)	$HC_2CH_2OH + H^+ \rightarrow HC_2CH_2OH_2^+ + H$	6.43×10^{-9}	-0.5	0.0	$3.86 \times 10^{-8} (1.46 \times 10^{-8})^x$	-
R22 (IN)	$HC_2CH_2OH + H_2D^+ \rightarrow HC_2CH_2OHD^+ + H_2$	3.21×10^{-9}	-0.5	0.0	$1.93 \times 10^{-8} (7.29 \times 10^{-9})^x$	-
R23 (IN)	$HC_2CHO + C^+ \rightarrow HC_3O^+ + CH$	3.80×10^{-9}	-0.5	0.0	$2.19 \times 10^{-8} (7.64 \times 10^{-9})^x$	-
R24 (IN)	$HC_2CHO + C^+ \rightarrow C_3H^+ + HCO$	3.80×10^{-9}	-0.5	0.0	$2.19 \times 10^{-8} (7.64 \times 10^{-9})^x$	-
R25 (IN)	$HC_2CHO + H_3O^+ \rightarrow HC_2CH_2O^+ + H_2O$	3.17×10^{-9}	-0.5	0.0	$1.83 \times 10^{-8} (6.38 \times 10^{-9})^x$	-
R26 (IN)	$HC_2CHO + HCO^+ \rightarrow HC_2CH_2O^+ + CO$	2.74×10^{-9}	-0.5	0.0	$1.58 \times 10^{-8} (5.51 \times 10^{-9})^x$	-
R27 (IN)	$HC_2CHO + H_3^+ \rightarrow C_3H^+ + H_2O + H_2$	7.03×10^{-9}	-0.5	0.0	$4.04 \times 10^{-8} (1.41 \times 10^{-8})^x$	-
R28 (IN)	$HC_2CHO + H_3^+ \rightarrow HC_2CH_2O^+ + H_2$	7.03×10^{-9}	-0.5	0.0	$4.04 \times 10^{-8} (1.41 \times 10^{-8})^x$	-
R29 (IN)	$HC_2CHO + He^+ \rightarrow C_3H^+ + He + OH$	6.17×10^{-9}	-0.5	0.0	$3.55 \times 10^{-8} (1.24 \times 10^{-8})^x$	-
R30 (IN)	$HC_2CHO + He^+ \rightarrow C_3H + He + OH^+$	6.17×10^{-9}	-0.5	0.0	$3.55 \times 10^{-8} (1.24 \times 10^{-8})^x$	-
R31 (IN)	$HC_2CHO + CH_3^+ \rightarrow HC_2CH_2O^+ + CH_2$	3.47×10^{-9}	-0.5	0.0	$2.00 \times 10^{-8} (6.98 \times 10^{-9})^x$	-
R32 (IN)	$HC_2CHO + H^+ \rightarrow C_3H^+ + H_2O$	1.20×10^{-8}	-0.5	0.0	$6.89 \times 10^{-8} (2.41 \times 10^{-8})^x$	-
R33 (IN)	$HC_2CHO + H^+ \rightarrow C_3H_2 + OH^+$	1.20×10^{-8}	-0.5	0.0	$6.89 \times 10^{-8} (2.41 \times 10^{-8})^x$	-
R34 (IN)	$HC_2CHO + H^+ \rightarrow HC_3O^+ + H_2$	1.20×10^{-8}	-0.5	0.0	$6.89 \times 10^{-8} (2.41 \times 10^{-8})^x$	-
R35 (IN)	$HC_2CHO + H^+ \rightarrow C_3O^+ + H_2$	1.20×10^{-8}	-0.5	0.0	$6.89 \times 10^{-8} (2.41 \times 10^{-8})^x$	-
R36 (IN)	$HC_2CHO + H_2D^+ \rightarrow HC_2CH_2O^+ + HD$	5.98×10^{-9}	-0.5	0.0	$3.44 \times 10^{-8} (1.20 \times 10^{-8})^x$	-
R37 (IN)	$HC_2CH_2O + C^+ \rightarrow HC_3O^+ + CH_2$	1.41×10^{-9}	-0.5	0.0	$8.86 \times 10^{-9} (3.57 \times 10^{-9})^x$	-
R38 (IN)	$HC_2CH_2O + C^+ \rightarrow C_3H_3^+ + HCO$	1.41×10^{-9}	-0.5	0.0	$8.86 \times 10^{-9} (3.57 \times 10^{-9})^x$	-
R39 (IN)	$HC_2CH_2O + H_3O^+ \rightarrow HC_2CH_2O^+ + H_2O$	1.18×10^{-9}	-0.5	0.0	$7.40 \times 10^{-9} (2.92 \times 10^{-9})^x$	-
R40 (IN)	$HC_2CH_2O + HCO^+ \rightarrow HC_2CH_2O^+ + HCO$	1.02×10^{-9}	-0.5	0.0	$6.38 \times 10^{-9} (2.58 \times 10^{-9})^x$	-
R41 (IN)	$HC_2CH_2O + H_3^+ \rightarrow C_3H_3^+ + H_2O + H_2$	2.62×10^{-9}	-0.5	0.0	$1.64 \times 10^{-8} (6.62 \times 10^{-9})^x$	-
R42 (IN)	$HC_2CH_2O + H_3^+ \rightarrow HC_2CH_2O^+ + H_2 + H$	2.62×10^{-9}	-0.5	0.0	$1.64 \times 10^{-8} (6.62 \times 10^{-9})^x$	-
R43 (IN)	$HC_2CH_2O + He^+ \rightarrow C_3H^+ + He + H_2O$	2.30×10^{-9}	-0.5	0.0	$1.44 \times 10^{-8} (5.80 \times 10^{-9})^x$	-
R44 (IN)	$HC_2CH_2O + He^+ \rightarrow C_4H + He + OH^+$	2.30×10^{-9}	-0.5	0.0	$1.44 \times 10^{-8} (5.80 \times 10^{-9})^x$	-
R45 (IN)	$HC_2CH_2O + CH_3^+ \rightarrow HC_2CH_2O^+ + CH_3$	1.29×10^{-9}	-0.5	0.0	$8.09 \times 10^{-9} (3.26 \times 10^{-9})^x$	-
R46 (IN)	$HC_2CH_2O + H^+ \rightarrow C_3H_3^+ + H_2O$	4.46×10^{-9}	-0.5	0.0	$2.80 \times 10^{-8} (1.13 \times 10^{-8})^x$	-
R47 (IN)	$HC_2CH_2O + H^+ \rightarrow C_3H_2 + OH^+ + H$	4.46×10^{-9}	-0.5	0.0	$2.80 \times 10^{-8} (1.13 \times 10^{-8})^x$	-
R48 (IN)	$HC_2CH_2O + H^+ \rightarrow HC_3O^+ + H_2 + H$	4.46×10^{-9}	-0.5	0.0	$2.80 \times 10^{-8} (1.13 \times 10^{-8})^x$	-
R49 (IN)	$HC_2CH_2O + H^+ \rightarrow HC_3O^+ + H_2$	4.46×10^{-9}	-0.5	0.0	$2.80 \times 10^{-8} (1.13 \times 10^{-8})^x$	-
R50 (IN)	$HC_2CH_2O + H_2D^+ \rightarrow HC_2CH_2O^+ + HD + H$	2.23×10^{-9}	-0.5	0.0	$1.40 \times 10^{-8} (5.63 \times 10^{-9})^x$	-
R51 (PH)	$HC_2CH_2OH + PHOTON \rightarrow C_3H_3 + OH$	6.0×10^{-10}	0.0	1.8	$9.14 \times 10^{-18} (9.14 \times 10^{-18})^y$	$9.14 \times 10^{-18} (9.14 \times 10^{-18})^y$
R52 (PH)	$HC_2CH_2OH + PHOTON \rightarrow HC_2CH_2O + H$	6.0×10^{-10}	0.0	1.8	$9.14 \times 10^{-18} (9.14 \times 10^{-18})^y$	$9.14 \times 10^{-18} (9.14 \times 10^{-18})^y$
R53 (PH)	$HC_2CH_2O + PHOTON \rightarrow C_3H_2 + OH$	6.0×10^{-10}	0.0	1.8	$9.14 \times 10^{-18} (9.14 \times 10^{-18})^y$	$9.14 \times 10^{-18} (9.14 \times 10^{-18})^y$
R54 (PH)	$HC_2CH_2O + PHOTON \rightarrow H_2CO + C_2H$	6.0×10^{-10}	0.0	1.8	$9.14 \times 10^{-18} (9.14 \times 10^{-18})^y$	$9.14 \times 10^{-18} (9.14 \times 10^{-18})^y$
R55 (PH)	$HC_2CH_2O + PHOTON \rightarrow HC_2CHO + H$	6.0×10^{-10}	0.0	1.8	$9.14 \times 10^{-18} (9.14 \times 10^{-18})^y$	$9.14 \times 10^{-18} (9.14 \times 10^{-18})^y$
R56 (PH)	$HC_2CHO + PHOTON \rightarrow C_3H + HCO$	6.0×10^{-10}	0.0	1.8	$9.14 \times 10^{-18} (9.14 \times 10^{-18})^y$	$9.14 \times 10^{-18} (9.14 \times 10^{-18})^y$
R57 (PH)	$HOC_2HHCHOH + PHOTON \rightarrow HC_2CH_2OH + OH$	6.0×10^{-10}	0.0	1.8	$9.14 \times 10^{-18} (9.14 \times 10^{-18})^y$	$9.14 \times 10^{-18} (9.14 \times 10^{-18})^y$
R58 (PH)	$HOC_2HHCHOD + PHOTON \rightarrow HC_2CH_2OH + OD$	6.0×10^{-10}	0.0	1.8	$9.14 \times 10^{-18} (9.14 \times 10^{-18})^y$	$9.14 \times 10^{-18} (9.14 \times 10^{-18})^y$
R59 (CR)	$HC_2CH_2OH + CRPHOT \rightarrow C_3H_3 + OH$	1.3×10^{-17}	0.0	752	$2.44 \times 10^{-14} (2.44 \times 10^{-14})^y$	$2.44 \times 10^{-14} (2.44 \times 10^{-14})^y$
R60 (CR)	$HC_2CH_2OH + CRPHOT \rightarrow HC_2CH_2O + H$	1.3×10^{-17}	0.0	752	$2.44 \times 10^{-14} (2.44 \times 10^{-14})^y$	$2.44 \times 10^{-14} (2.44 \times 10^{-14})^y$
R61 (CR)	$HC_2CH_2O + CRPHOT \rightarrow C_3H_2 + OH$	1.3×10^{-17}	0.0	752	$2.44 \times 10^{-14} (2.44 \times 10^{-14})^y$	$2.44 \times 10^{-14} (2.44 \times 10^{-14})^y$
R62 (CR)	$HC_2CH_2O + CRPHOT \rightarrow H_2CO + C_2H$	1.3×10^{-17}	0.0	752	$2.44 \times 10^{-14} (2.44 \times 10^{-14})^y$	$2.44 \times 10^{-14} (2.44 \times 10^{-14})^y$
R63 (CR)	$HC_2CH_2O + CRPHOT \rightarrow HC_2CHO + H$	1.3×10^{-17}	0.0	752	$2.44 \times 10^{-14} (2.44 \times 10^{-14})^y$	$2.44 \times 10^{-14} (2.44 \times 10^{-14})^y$
R64 (CR)	$HC_2CHO + CRPHOT \rightarrow C_2H + HCO$	1.3×10^{-17}	0.0	752	$2.44 \times 10^{-14} (2.44 \times 10^{-14})^y$	$2.44 \times 10^{-14} (2.44 \times 10^{-14})^y$
R65 (CR)	$HOC_2HHCHOH + CRPHOT \rightarrow HC_2CH_2OH + OH$	1.3×10^{-17}	0.0	752	$2.44 \times 10^{-14} (2.44 \times 10^{-14})^y$	$2.44 \times 10^{-14} (2.44 \times 10^{-14})^y$
R66 (CR)	$HOC_2HHCHOD + CRPHOT \rightarrow HC_2CH_2OH + OD$	1.3×10^{-17}	0.0	752	$2.44 \times 10^{-14} (2.44 \times 10^{-14})^y$	$2.44 \times 10^{-14} (2.44 \times 10^{-14})^y$
R67 (DR)	$HC_2CH_2O^+ + e^- \rightarrow CO + C_2H_2 + H$	2.0×10^{-7}	-0.5	0.0	$1.10 \times 10^{-6} (3.46 \times 10^{-7})^x$	-
R68 (DR)	$HC_2CH_2O^+ + e^- \rightarrow HCO + C_2H + H$	2.0×10^{-7}	-0.5	0.0	$1.10 \times 10^{-6} (3.46 \times 10^{-7})^x$	-
R69 (DR)	$HC_2CH_2O^+ + e^- \rightarrow H_2CO + C_2H$	2.0×10^{-7}	-0.5	0.0	$1.10 \times 10^{-6} (3.46 \times 10^{-7})^x$	-
R70 (DR)	$HC_2CH_2OH_2^+ + e^- \rightarrow C_3H_3 + H_2O$	8.01×10^{-8}	-0.59	0.0	$5.95 \times 10^{-7} (1.52 \times 10^{-7})^x$	-
R71 (DR)	$HC_2CH_2OH_2^+ + e^- \rightarrow C_3H_3 + OH + H$	4.54×10^{-7}	-0.59	0.0	$3.34 \times 10^{-6} (8.6 \times 10^{-7})^x$	-
R72 (DR)	$HC_2CH_2OH_2^+ + e^- \rightarrow C_3H_2 + H_2O + H$	1.87×10^{-7}	-0.59	0.0	$1.41 \times 10^{-6} (3.63 \times 10^{-7})^x$	-
R73 (DR)	$HC_2CH_2OH_2^+ + e^- \rightarrow H_2CO + C_2H_2 + H$	8.9×10^{-8}	-0.59	0.0	$6.6 \times 10^{-7} (1.7 \times 10^{-7})^x$	-
R74 (DR)	$HC_2CH_2OH^+ + e^- \rightarrow C_3H_3 + OH$	3.00×10^{-7}	-0.5	0.0	$1.64 \times 10^{-6} (5.20 \times 10^{-7})^x$	-
R75 (DR)	$HC_2CH_2OH^+ + e^- \rightarrow HC_2CH_2O + H$	3.00×10^{-7}	-0.5	0.0	$1.64 \times 10^{-6} (5.20 \times 10^{-7})^x$	-

Notes: For the two-body reactions (R1-R2, R4-R8, R67-R75), rate coefficients are tabulated as $\alpha \left(\frac{T}{300}\right)^\beta \exp(-\frac{\gamma}{T})$. For the photo-dissociation reactions with external interstellar photons (R51-R58), rate coefficients are tabulated as $\alpha \exp(-\gamma A_V)$. For photo-dissociation by cosmic ray induced photons (R59-R66), rate coefficients are tabulated as $\alpha \frac{J_{\gamma}}{1-\omega}$. For the rate coefficients of ion-polar neutral reactions (R9-R50), we use the relation discussed in Su & Chesnavich (1982).

Tabulated rate coefficients for these ion-neutral reactions in terms of $\alpha \left(\frac{T}{300}\right)^\beta \exp(-\frac{\gamma}{T})$ are valid for the low temperature regime only.

^a gas phase enthalpy in kJ/mol

^b ice phase enthalpy in kJ/mol

^x rate coefficient in $\text{cm}^3 \text{s}^{-1}$

^y rate coefficient in s^{-1}

propynal and H_2O are found to be highly endothermic in nature whereas reaction R5 is highly exothermic and is likely barrier-less, since the reactants are both radicals. Since both reactants in R5 (C_3H_3 and OH) are reasonably abundant in the ISM, we think that this reaction can contribute towards the formation of interstellar PA, although, in the gas phase, it must proceed via a radiative route, so that it must be looked at closely. On ice mantles, however, radical-radical association reactions are normally quite efficient. As can be seen in Table 1, R4 and R5 are the sole radical-radical reactions leading directly to the formation of PA, both in the gas and on the ice. A gas phase dissociative recombination (DR) reaction (R6), in which protonated PA and an electron recombine to form smaller neutral products, is also included. This reaction may contribute significantly to the gas phase formation of PA unless the two-body product channel shown is unimportant if ion-neutral processes can produce protonated PA efficiently. Similar pathways to all those considered for the synthesis of PA are assumed to be responsible for the production of OD-PA.

2.2. Destruction pathways

As shown in Table 1, the destruction of gaseous PA occurs via ion-neutral (IN) and photo-dissociative (PH & CR) pathways, as well as via two radical-neutral (NR) reactions. The destruction of gas phase PA also occurs via adsorption onto ice, but the reverse process of desorption also occurs. These processes are in our network, but not listed in Table 1. The rate coefficient for the gas phase NR reaction between the hydroxyl radical (OH) and PA was measured by Upadhyaya et al. (2001), who used laser photolysis combined with the laser induced fluorescence technique at room temperature. According to their study, this reaction (R7) produces an adduct, $\text{HOC}_2\text{HHCHOH}$. Since the abundances of OH and OD are comparable in a dense cloud (Millar et al., 1989), a similar destruction mechanism with OD (R8) is also considered here. In addition to the gas-phase, reactions R7 and R8 are included in the ice phase as well. For the ion-neutral (IN) destruction of gas phase PA, we include reactions R9-R22 by following the similar gas phase ion-neutral (IN) destruction pathways available for methanol in Woodall et al. (2007). Similar IN destruction reactions (R23-R50) for HC_2CHO and $\text{HC}_2\text{CH}_2\text{O}$ are also considered. Photo-dissociation reactions (direct or cosmic ray induced) (R51-R66) are also responsible for the destruction of PA and its associated species in both phases. In Table 1, DR reactions R6 and R67-R75 involve the ions ($\text{HC}_2\text{CH}_2\text{O}^+$, $\text{HC}_2\text{CH}_2\text{OH}_2^+$ and $\text{HC}_2\text{CH}_2\text{OH}^+$); these ions are produced by various formation/destruction pathways of PA and its related species. For the destruction of OD-PA and other associated species similar destruction pathways to all those considered for PA are included.

2.3. Rate coefficients

2.3.1. Gas phase rate coefficients

Slagle et al. (1991) experimentally obtained a temperature independent rate coefficient of $\sim 2.31 \times 10^{-10} \text{ cm}^3 \text{ s}^{-1}$ for reaction R1. According to their study, this reaction proceeds through a fast and irreversible association-fragmentation process. We utilize the rate coefficient obtained by Slagle et al. (1991). Petrie

(1995) estimated a rate coefficient of $1.0 \times 10^{-10} \text{ cm}^3 \text{ s}^{-1}$ for reaction R2 with the assumption that it occurs without a barrier in the gas phase. Although this assumption contradicts the calculation of a small barrier by Dong et al. (2005), we assume the reaction to be barrier-less, and use the estimated rate coefficient of Petrie (1995).

As can be seen in Table 1, reactions R3, R4, and R5 are highly exothermic in nature. Based on the high exothermicity of these reactions, one might assume that these reactions can process without barriers.

The Hydrogen addition reaction of HC_2CHO (reaction R3) may occur in two ways. First, H addition may occur with the O atom of the CHO group and produce HC_2CHOH and secondly H addition may occur with the C atom of the CHO group and produce $\text{HC}_2\text{CH}_2\text{O}$. Our quantum chemical calculation found that the hydrogen addition to carbon is more favourable than the hydrogen addition to oxygen in the CHO group. Using the DFT/6-31+G(d,p) method, we found that the gas-phase activation barrier (ΔE^\ddagger) and Gibbs energy of activation (ΔG^\ddagger) for the second possibility of reaction R3 ($\text{H} + \text{HC}_2\text{CHO} \rightarrow \text{HC}_2\text{CH}_2\text{O}$) is 3.74 kcal/mol and 9.63 kcal/mol respectively.

For the computation of the gas phase rate coefficient for reaction R3, we use transition state theory, which leads to the Eyring equation (Eyring, 1935):

$$k = (k_B T / hc) \exp(-\Delta G^\ddagger / RT). \quad (1)$$

The rate coefficient calculated by the above equation thus has a strong temperature dependence. In Table 1, we have included the rate coefficient for two temperatures; 10 K and 100 K. At 10 K, rate coefficient is ~ 0 and at 100 K it becomes $1.96 \times 10^{-15} \text{ cm}^3 \text{ s}^{-1}$. Thus in the low temperature regime, R3 does not contribute at all to the gas phase formation of PA, while it could play a role for the formation of PA in the high temperature regime.

In the case of reactions R4 and R5, we were unable to locate any suitable transition state and assume that these two reactions are barrier-less, as is customary for radical-radical reactions. The rate coefficients of these two reactions are assumed to be $10^{-10} \text{ cm}^3 \text{ s}^{-1}$. The formation of OD-PA is treated with similar pathways and rate coefficients.

For the formation of PA by the DR mechanism, which involves the destruction of $\text{HC}_2\text{CH}_2\text{OH}_2^+$ (R6, R67-R75), we follow the destruction of CH_3OH_2^+ from Woodall et al. (2007) for the rate coefficients and product channels. Rate coefficients between two species are standardly parameterized as a function of temperature by the equation

$$k = \alpha(T/300)^\beta \exp^{-\gamma/T}. \quad (2)$$

In this particular case, the values of the parameters for the formation of PA are $\alpha = 2.67 \times 10^{-8} \text{ cm}^3 \text{ s}^{-1}$, $\beta = -0.59$ and $\gamma = 0$. Similar product channels and rate coefficients are used for the formation of OD-PA by a DR reaction.

Now let us consider the destruction of gaseous PA. Upadhyaya et al. (2001) studied the rate coefficient of the NR reaction between PA and the OH radical (R7). According to

their study, it produces an adduct with a rate coefficient of $(9.2 \pm 1.4) \times 10^{-12} \text{ cm}^3 \text{ s}^{-1}$, which we use with no temperature dependence. Here also, we assume a similar rate coefficient for reaction R8, which involves OD. Similar destruction reactions and rate coefficients are adopted for OD-PA as well.

Ion Neutral (IN) reactions are the dominant means for the destruction of neutral interstellar species. If the neutral species is non-polar, we use the Langevin collision rate coefficient (Herbst, 2006; Wakelam et al., 2010). If the neutral species is polar, we employ the trajectory scaling relation found in Su & Chesnavich (1982) and Woon & Herbst (2009). From our quantum chemical calculations, we find that the polarizability $\alpha_d = 5.62 \times 10^{-24} \text{ cm}^3$ and dipole moment $\mu_D = 1.6548$ Debye for PA. For the destruction reactions of the other two associated species (HC_2CHO , $\text{HC}_2\text{CH}_2\text{O}$), in reaction numbers R23-R36, we use $\alpha_d = 5.26 \times 10^{-24} \text{ cm}^3$ and $\mu_D = 3.08$ Debye, and for R37-R50 we use $\alpha_d = 5.93 \times 10^{-24} \text{ cm}^3$ and $\mu_D = 1.1480$ Debye. For deuterated PA, the ion-neutral destruction reactions have similar rate coefficients to those of normal PA, the only differences being due to the reduced mass, which are rather small. Deuterated reactions and their rate coefficients are not tabulated here.

For the photo-dissociation reactions of PA and its associated species by external interstellar photons and cosmic ray-induced photons, we use analogous products and the same first-order rate coefficients (s^{-1}) as the case of CH_3OH (Woodall et al., 2007). For the case of external photons, we use the following relation for the rate coefficients:

$$k = \alpha \exp(-\gamma A_V) \quad (3)$$

where α represents the rate coefficient (s^{-1}) in the unshielded interstellar ultraviolet radiation field, A_V is the visual extinction, for which we use a value of 10, and γ is used to take into account the increased extinction of dust in the UV. Here, following Woodall et al. (2007), we use $\alpha = 6.0 \times 10^{-10} \text{ s}^{-1}$, and $\gamma = 1.8$ in our model. Incorporating all the parameters into the above equation, we obtain a photo-dissociation rate coefficient of about $9.14 \times 10^{-18} \text{ s}^{-1}$.

For cosmic-ray-induced photo-reactions, we use the following relation, which was originally developed by (Gredel et al., 1989):

$$k = \alpha \gamma' / (1 - \omega) \quad (4)$$

where α is the cosmic-ray ionization rate (s^{-1}), γ' is the number of photo-dissociative events that take place per cosmic-ray ionization and ω is the dust grain albedo in the far ultraviolet. Here, we use $\omega = 0.6$, $\alpha = 1.3 \times 10^{-17} \text{ s}^{-1}$, and $\gamma' = 752.0$ by following the cosmic-ray-induced photo-reactions of CH_3OH in Woodall et al. (2007). By including these parameters into the above equation, we obtain a rate coefficient of $2.44 \times 10^{-14} \text{ s}^{-1}$, which is roughly 4 orders higher than the rate of external photo-dissociative reactions. Cosmic ray induced photo-reactions can play an important role in interstellar chemistry. The choices of these parameters are highly reaction specific and a wrong estimation might lead to misleading results. In the UMIST 2006 database, γ' ranges as high as 5290 and as low as 25.0. Though the higher values of γ' are more reliable for the larger molecules

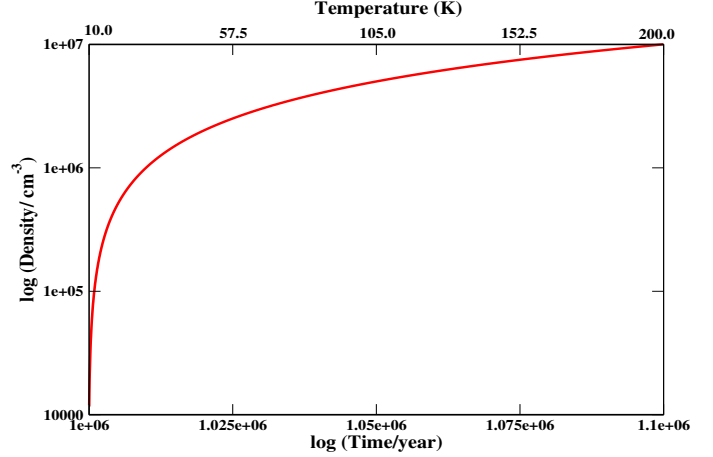


Figure 1: Adopted physical conditions for the warm-up phase in which the density increases as the temperature increases. .

because of the increasing overlap between the cross sections for photo-dissociation and the cosmic-ray-induced emission spectrum (Gredel et al., 1989), we use $\gamma' = 752.0$ (in Table 1, we presented it under the column head marked γ) for our calculations of the cosmic-ray-induced photo-dissociative reactions. The same photo-dissociation rate coefficients are adopted for the destruction of OD-PA and its associated species.

Dissociative recombination (DR) reactions and rate coefficients for some of the associated ions of PA are shown in reactions R67-R75. Pathways and rate coefficients of these reactions are adopted by following the similar DR pathways available for CH_3O^+ , CH_3OH_2^+ , and CH_3OH^+ in Woodall et al. (2007). Since for all these reactions, $\beta \neq 0$, the reactions are temperature dependent. The same DR rate coefficients are used for the associated ions of OD-PA.

For two or three-body gas-phase reactions in Table 1, the rate coefficients are represented in terms of the three rate coefficients, α , β and γ . Most of the gas phase rate coefficients adopted here are either estimated or taken from similar kind of reactions. For reactions R1-R2, R4-R5 and R7-R8, we assign β and γ to be zero. For the dissociative recombination reactions (R6 and R68-R75), these three coefficients are estimated based on similar reactions listed in Woodall et al. (2007). For reaction R3, we calculate the gas phase rate coefficient by using transition state theory, which leads to the Eyring equation (Eyring, 1935). Thus for reaction R3, these three parameters are not shown. For destruction by photo-reactions, we supply these three coefficients following the similar type of reactions available in Woodall et al. (2007). For the destruction of polar neutral species by ions, we use the two relations discussed in Su & Chesnavich (1982). These relations cannot be represented over the whole temperature range in terms of one set of three coefficients. However, we can tabulate α , β and γ for reactions R9-R50 in the low temperature regime.

2.3.2. Ice phase rate coefficients

Chemical enrichment of interstellar grain mantles depends on the binding energies (E_d) and barriers against diffusion

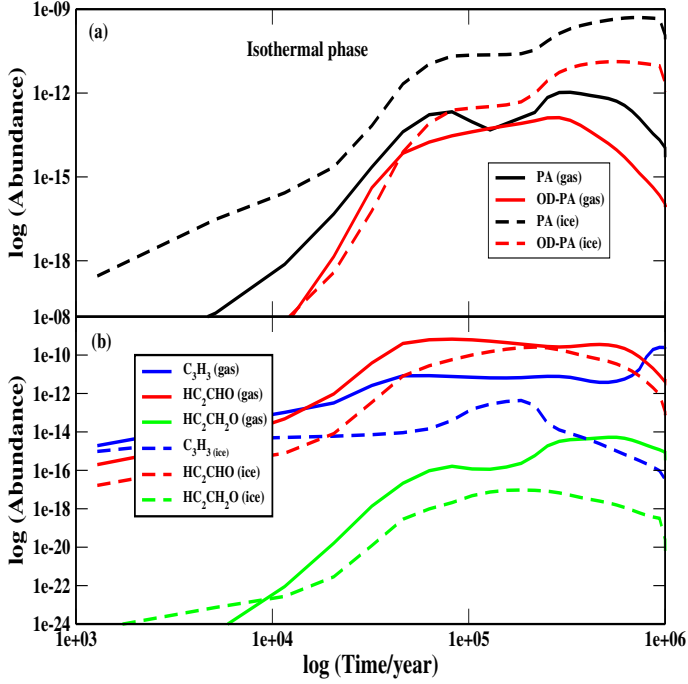


Figure 2: Chemical evolution of (a) PA and OD-PA and (b) their related species during the isothermal phase at $n_H = 10^4 \text{ cm}^{-3}$ with a constant visual extinction of 10.

(E_b) of the adsorbed species. The binding energies of these species are often available from past studies (Allen & Robinson, 1977; Tielens & Allamandola, 1987; Hasegawa & Herbst, 1993; Hasegawa et al., 1992). But these binding energies mostly pertain to silicates. Binding energies of the most important surface species on ice, which mostly control the chemical composition of interstellar grain mantles, are available from some recent studies (Cuppen & Herbst, 2007; Garrod, 2013). We use these latter energies in our model. For the rest of the species for which binding energies are still unavailable, we use the same values as in past studies or estimate new values. For barriers against diffusion, which are poorly known, we use values equal to $0.35E_d$ (Garrod, 2013).

For the formation of PA in the ice phase, we include surface reactions R1-R5. The rate coefficients (R_{diff}) of these reactions were calculated by the method described in Hasegawa et al. (1992), which is based on thermal diffusion. They defined a probability factor κ to differentiate between exothermic reactions without activation energy barriers and reactions with activation energy barriers (E_a) in such a way that the effective rate coefficient becomes $R_{ij} = \kappa \times R_{diff}$. The factor κ is unity in the absence of a barrier. For reactions with activation energy barriers, κ is defined as the quantum mechanical probability for tunneling through a rectangular barrier of thickness $a (= 1 \text{ \AA})$, which is calculated from the equation

$$\kappa = \exp[-2(a/\hbar)(2\mu E_a)^{1/2}]. \quad (5)$$

Binding energies to the surface for some complex organics with a hydroxyl group are normally considered to be higher due to the phenomenon of hydrogen bonding (Collings et al.,

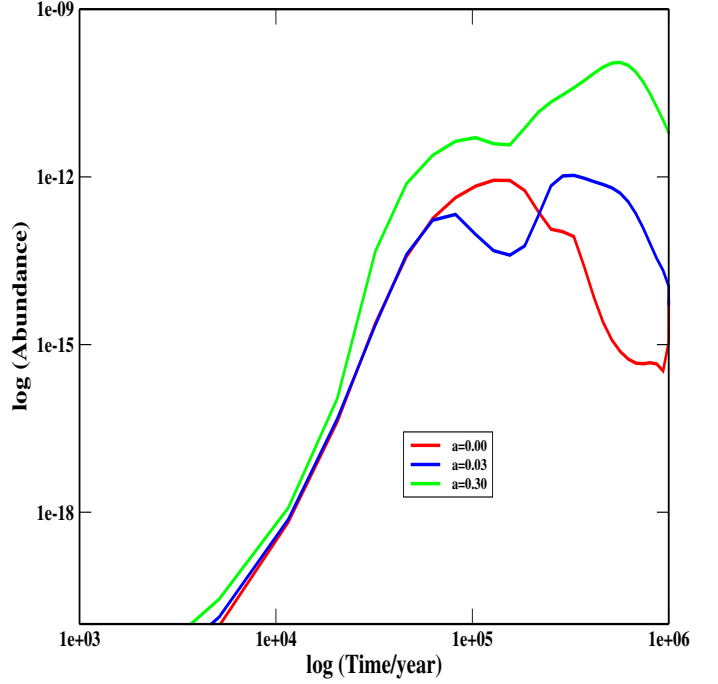


Figure 3: Chemical evolution of PA during the constant density isothermal phase at $n_H = 10^4 \text{ cm}^{-3}$ with a constant visual extinction of 10 and different values of the non-thermal reactive desorption parameter a .

2004; Lattalais et al., 2011; Garrod, 2013). Since PA has an -OH group, creating hydrogen bonds with a water substrate, this molecule is therefore expected to have a higher binding energy, close to that of water. Here, we assume the binding energy of both PA and OD-PA to be the same as methanol (5530 K). Since HC_2CHO forms by the reaction between C_3H_3 and O, we add the binding energies of C_3H_3 (2220 K) and O (800 K) to determine a binding energy value 3020 K. In the case of the binding energy of $\text{HC}_2\text{CH}_2\text{O}$, we add the binding energies of HC_2CHO (3020 K) and H (450 K) to obtain 3470 K. For other binding energies for species in reaction R1, R2, R3, R4 and R5, we use $E_d(\text{C}_2\text{H}) = 1460 \text{ K}$, $E_d(\text{H}_2\text{CO}) = 2050 \text{ K}$ and $E_d(\text{OH}) = 2850 \text{ K}$. Our transition state theory calculation found that reaction R3 (hydrogen addition to the carbon atom of the CHO group) contains an activation barrier of about 3.59 kcal/mol (1807 K) in the ice phase.

Destruction of ice phase PA occurs by various means; thermal desorption, non-thermal desorption from interstellar dust grains via exothermic surface reactions, cosmic ray induced desorption, photo-dissociation, and reaction with OH or OD radicals. Intact photo-desorption is not included. Thermal desorption plays a crucial role only at high temperatures, depending upon the adsorbed species. For thermal desorption, we use the relation prescribed by Hasegawa et al. (1992). At low temperatures, non-thermal desorption by reaction exothermicity, photons, and cosmic rays serve as important means for transferring the surface molecules to the gas phase. For non-thermal reactive desorption (Garrod & Herbst, 2006), we consider that all surface reactions which result in a single product break the surface-molecule bond with some fraction a . Here, we use a

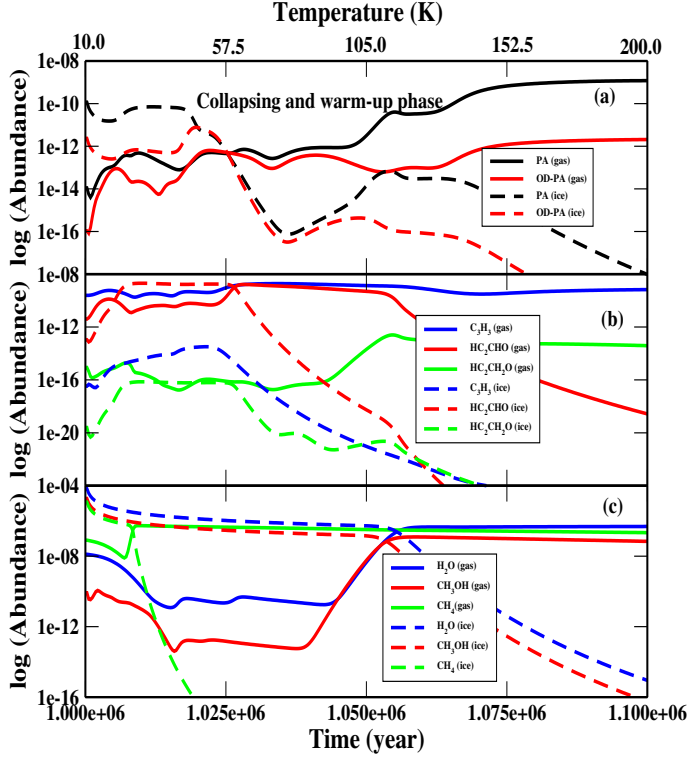


Figure 4: Chemical evolution of (a) PA and OD-PA (b) C_3H_3 , HC_2CHO and HC_2CH_2O (c) H_2O , CH_3OH and CH_4 for the warm-up phase, during which both density and temperature increase.

fiducial value for the fraction of $a = 0.03$. For the cosmic ray induced desorption rates, we follow the expression developed by Hasegawa & Herbst (1993). Photo-dissociation by direct (R51-R58) as well as cosmic ray induced photons (R59-R66) are considered for the destruction of ice phase PA and its two associated species, and the rate coefficients were assumed similar to their gas phase rate coefficients. The dissociated products remain on the grain surface and are thus able to react and desorb depending on their binding energies. For the destruction of ice phase PA by reactions with OH and OD (R7 and R8), we consider the destruction pathways proposed by Upadhyaya et al. (2001) for the gas-phase, but we calculate the rate coefficients of these ice phase reaction pathways by using diffusive reactions with barriers against diffusion, which have already been discussed. Selected ice phase rate coefficients used for PA are shown in Table 1 for $T = 10$ K and 100 K. Desorption and accretion rate coefficients are not included.

3. Chemical modeling

3.1. Model

We use our large gas-grain chemical network (Das et al., 2015a,b) for the purpose of chemical modeling. We assume that the gas and grains are coupled through accretion and thermal and non-thermal desorption processes. A visual extinction of 10 and a cosmic ray ionization rate of $1.3 \times 10^{-17} \text{ s}^{-1}$ are used. Including the deuterated reactions and deuterated species, our present gas phase chemical network consists of

6384 reactions involving 641 gas phase species and the surface chemical network consists of 358 reactions involving 291 surface species. The gas phase chemical network is mainly adopted from the UMIST 2006 database (Woodall et al., 2007), but contains some deuterated reactions as well. To minimize the huge computational time and avoid difficulty in handling a large chemical network, we have considered only some dominant deuterated reaction pathways. Deuteration reactions important for the increase of deuteration in the cold gas phase are included in our network. Our selection was based on some earlier studies by Rodgers & Millar (1996); Roberts & Millar (2000); Roberts et al. (2003). All the deuterated reactions, which were added/updated and identified as the dominant pathways for the formation of essential deuterated species in the tables (Table 13-18) of Albertsson et al. (2013) are also included here. For the grain surface reaction network, we primarily follow Hasegawa et al. (1992) and Cuppen & Herbst (2007), while for the ice phase deuterium fractionation reactions, we follow Caselli (2002) and Cazaux et al. (2012). In addition to this, we consider some reactions involving PA and coupled species, which are described in Section 2.

Initial elemental abundances with respect to total H nuclei in all forms are shown in Table 2. These “low metal” abundances are often used for dense clouds, where hydrogen is mostly in the form of molecular hydrogen and ionization of the medium is mainly governed by cosmic rays. We adopted these values from Leung et al. (1984). It is assumed that initially all deuterium is locked up in the form of HD. The initial abundance of HD is assumed to be 1.6×10^{-5} (Roberts & Millar, 2000) with respect to the total number of hydrogen nuclei.

In order to consider suitable physical conditions for a star forming region, we adopt a model with an initial phase of constant density ($n_H = 1.0 \times 10^4 \text{ cm}^{-3}$) and temperature ($T = 10$ K) followed by a warm-up phase (temperature increases from 10 K to 200 K). The warm-up phase is assumed to be accompanied by an increase of density from $n_H = 10^4 \text{ cm}^{-3}$ to $n_H = 10^7 \text{ cm}^{-3}$, relevant when the material approaches the inner protostellar regions and appropriate for hot-core conditions. Both phases have a visual extinction of 10. The initial phase is assumed to be sustained for 10^6 years and the subsequent phase lasts for another 10^5 years (a typical lifetime for a young embedded stage (Evans et al., 2009)). In Fig. 1, the adopted time-dependent physical conditions for the second stage of evolution are shown.

For the rise in density and temperature, we assume constant slopes m_{den} and m_{temp} respectively for the density and temperature as determined from the following equations:

$$m_{\text{den}} = \frac{\rho_{\text{max}} - \rho_{\text{min}}}{\text{Time}_f - \text{Time}_i} = 99.9 \text{ cm}^{-3} \text{ yr}^{-1}, \quad (6)$$

$$m_{\text{temp}} = \frac{T_{\text{max}} - T_{\text{min}}}{\text{Time}_f - \text{Time}_i} = 1.9 \times 10^{-3} \text{ K yr}^{-1}. \quad (7)$$

3.2. Modeling Results

Figure 2a,b shows the chemical evolution of PA, OD-PA and their related species in the gaseous (solid line) and ice phase

Table 2: Initial elemental abundances with respect to total hydrogen nuclei.

Species	Abundance
H ₂	5.00×10^{-01}
He	1.40×10^{-01}
N	2.14×10^{-05}
O	1.76×10^{-04}
e ⁻	7.31×10^{-05}
C ⁺	7.30×10^{-05}
S ⁺	8.00×10^{-08}
Si ⁺	8.00×10^{-09}
Fe ⁺	3.00×10^{-09}
Na ⁺	2.00×10^{-09}
Mg ⁺	7.00×10^{-09}
HD	1.6×10^{-05}

(dashed line) during the cold isothermal phase. The ice phase production of PA is dominated by the successive H association reactions (R3 and R4). Similarly, for the case of OD-PA, the association reactions are found to be dominant. The peak abundances of PA and OD-PA and their related species are listed in Table 3, for both phases of our calculation. For example, in the isothermal cold phase, the peak fractional abundances of PA and OD-PA in the ice p are 5.03×10^{-10} and 1.33×10^{-11} respectively and for the gas phase, these values are 1.07×10^{-12} and 1.32×10^{-13} . Note that the ice and gas phase peaks do not occur at the same time.

Non-thermal desorption processes significantly contribute to the maintenance of the gas-phase abundances of PA and OD-PA with our fiducial value a of 0.03 for reactive desorption. Fig. 3 show the gas phase abundance of PA versus time with $a = 0$, $a = 0.03$ and $a = 0.3$ in the isothermal phase. For the case of Fig. 3, throughout some but not all of the time of the evolutionary stage, the PA abundance for the $a = 0.03$ case is slightly higher than in the case without reactive desorption ($a = 0$). For the highest ‘ a ’ value ($a = 0.3$), with the most rapid reactive desorption, the gas phase peak abundance is significantly larger than that with $a = 0.03$ and also with $a = 0$. In the isothermal phase, the peak abundance of gas phase PA for these three values of a is found to be 8.69×10^{-13} , 1.07×10^{-12} and 1.12×10^{-10} for $a = 0.00$, 0.03 and 0.30 respectively. At the initial stages of evolution, the models with $a = 0$ and $a = 0.03$ give very similar gas phase abundances. This means that the gas phase production of PA in our fiducial model is actually dominated by gas phase chemistry (by reaction R5) as long as the a parameter is not too high.

Figure 4a,b,c refers to the warm-up portion of our simulation. Fig. 4a represents the evolution of PA and OD-PA whereas Fig. 4b represents the evolution of PA related species such as C₃H₃, HC₂CHO and HC₂CH₂O and Fig. 4c represents the evolution of the major icy species water, methane and methanol for the gas and ice phases. The temporal evolution of gas phase and ice species shown in Fig. 4a,b,c appears to differ slightly with similar models found in Garrod, Weaver & Herbst (2008). This difference is solely due to the adopted physical condition mentioned in section 3.1 in comparison to that in Garrod, Weaver & Herbst (2008). From Fig. 4c it is clear that among the main icy species, methane disappears first from the grain mantle due to its low adsorption energy (1300 K) followed by methanol (adsorption energy 5530 K) and water (adsorption energy 5700

K).

As can be seen, the gas phase production of PA and OD-PA is found to be favourable around the high temperature region. This happens due to the increase in the rate coefficient of reaction R3 with the temperature. For the ice phase reactions, H or D addition reactions become irrelevant beyond 40 K, beyond which the C₃H₃ and OH or OD radicals become mobile enough to react with each other on grain surfaces. At the same time, the destruction of PA and OD-PA by reactions with OH and OD increases due to the increase in the destruction rates with increasing temperature. Above 100 K, C₃H₃ and OH or OD radicals roughly disappear and the only source of ice phase PA or OD-PA is accretion from the gas phase. Since the density increases with time, accretion of the gas phase species becomes more favourable. Above 140 K, the gas phase abundances of PA and OD-PA are roughly invariant.

In Table 3, we list the peak abundances of PA, OD-PA and their related species for the warm-up phase along with their corresponding times and temperatures. In this phase, the peak abundances of ice phase PA and OD-PA are found to be decreased in comparison with the isothermal phase. The peak fractional abundances of ice phase PA and OD-PA are found to be 7.09×10^{-11} at 32.2 K, and 7.23×10^{-12} at 47.3 K, respectively, whereas, for the gas phase, the corresponding peak abundances are 1.20×10^{-9} and 2.14×10^{-12} respectively.

Although reality is more complex due to the consideration of variable density and temperature in the second phase, the basic explanation for the higher abundances of PA and OD-PA in the gas phase is that instead of chemical desorption, thermal desorption becomes much larger at higher temperatures, and indeed the ice abundances become infinitesimal at temperatures above 100 K. In the first phase of our simulation (Fig. 2), which occurs while the temperature is 10 K, only non-thermal slow desorption occurs, and indeed the ice abundances are higher.

For the gas-phase at higher temperatures, at which there is very little ice, fractionation occurs via gas-phase formation and destruction reactions, which lead to low fractionation at temperatures above 50 K due to endothermic reactions between selected deuterated ions with H₂ which return deuterated species to normal ones. After all, the high temperature limit of OD-PA/PA is 10^{-4} , which is close to the D/H elemental value of 10^{-5} . At temperatures under 50 K, the abundance ratio of gaseous OD-PA/PA approaches unity, a very high degree of fractionation, while the ice ratio is 10^{-2} . These high ratios prob-

ably stem from large values of the atomic abundance ratio D/H in the gas and on the grains at low temperatures.

In the warm-up case, the predicted fractional abundance of PA under hot-core conditions lies at approximately 10^{-9} . Our results argue strongly for the possibility of detection, especially at temperatures above 150 K. Interestingly, this prediction implies that PA does not occupy the same regions as does its isomer propenal. (Requena et al. (2008) measured its abundance to $\sim 2.30 \times 10^{-9}$ with respect to H_2), but the species is seen in absorption against Sgr B2(N), and so is more likely to be present in colder foreground gas (Hollis et al., 2004). For OD-PA, the predicted hot-core abundance is $\approx 10^{-12}$ at temperatures above 150. For the cold core case, even the peak fractional abundance of gas phase PA with the fiducial value of a is sufficiently low to rule out detection unless the highest value of the parameter a for reactive desorption is used. We conclude that PA and possibly OD-PA can most likely be detected in warm-up regions at temperatures above 100 K.

4. Astronomical Spectroscopy

4.1. Detectability of PA and OD-PA in the millimeter-wave regime

To estimate the possibility of detecting PA and OD-PA with present astronomical facilities, we use the CASSIS radiative transfer model [http://cassis.irap.omp.eu] at LTE with the JPL molecular database [http://spec.jpl.nasa.gov]. Propenal (CH_2CHCHO) had already been successfully detected towards the high mass star forming region Sagittarius B2(N) with the 100-meter Green Bank Telescope operating in the frequency range 18 – 26 GHz by Hollis et al. (2004). They had detected the $2_{11} - 1_{10}$ line of CH_2CHCHO with 14 mK intensity ($\approx 7\sigma$ detection). From our chemical model, we found that the peak abundances for PA and OD-PA are respectively 1.2×10^{-9} and 2.14×10^{-12} with respect to H_2 and for propenal, we use an abundance of 2.3×10^{-9} with respect to H_2 (Requena et al., 2008). As the input parameters, we use the following parameters, which represent a typical high mass star forming region analogous to Sgr B2 (N):

Column density of $H_2 = 10^{24} \text{ cm}^{-2}$,
Excitation temperature (T_{ex}) = 100 K,
FWHM = 5 km/s,
 $V_{\text{LSR}} = 74 \text{ km/s}$,
Source size to take into account the beam dilution = $3''$

From our radiative transfer model, the intensity for $2_{11} - 1_{10}$ line (18.28065 GHz) of PA is found to be 0.011 mK, which is far below than the detection limit of GBT ($3\sigma \approx 6 \text{ mK}$). Because of the higher dipole moment components of propenal ($\mu_a = 3.052 \text{ D}$, $\mu_b = 0.630 \text{ D}$ and $\mu_c = 0 \text{ D}$) compared with PA ($\mu_a = 1.037 \text{ D}$, $\mu_b = 0.147 \text{ D}$ and $\mu_c = 0.75 \text{ D}$), intensity of PA is much lower compared with propenal. This prompted us to suggest the use of high-spatial and high-spectral resolution observations from the Atacama Large Millimeter/Submillimeter Array (ALMA). In particular, we can use lower frequency bands of ALMA – Bands 1, 2 and 3 (31 – 116 GHz)

– since the observed rotational spectra for PA and OD-PA are expected to be cleaner in these frequency ranges given that low energy transitions of light molecules fall at much higher frequencies. This is why we have listed only the intense transitions for PA along with OD PA in Table 4 that fall in ALMA Bands 1, 2 and 3.

Currently ALMA Band 3 is in operation while Bands 1 and 2 are not yet available. The strongest transitions pointed out in Table 4 for PA (at 116.23546 GHz and 116.23586 GHz) are just beyond ALMA Band 3 and are not available in the ALMA time estimator. Thus, we have focused on the next strongest transitions of Band 3 at 89.39184 GHz and 89.39212 GHz, which also have an overlap with Band 2. Using Band 3, we can detect these transitions of PA with approximately 7.5 hours of integration time by assuming a spectral resolution of 0.5 km/s, a sensitivity of 17 mK, a signal-to-noise ratio of 6, an angular resolution 3 arcseconds and 40 antennas of 12 meter array in the ALMA time estimator. But it is not possible to detect any lines for OD-PA using ALMA Band 3 with any reasonable integration time.

4.2. Vibrational spectra

Here we use the MP2 method with an aug-cc-pVTZ basis set for the computation of the vibrational transition frequencies and intensities of various normal modes of vibration of PA and OD-PA. The prefix aug stands for diffuse functions and cc-pVTZ refers to Peterson and Dunnings correlation consistent basis set (Peterson & Dunning, 2002) for performing our calculations. The influence of the solvent in vibrational spectroscopy is taken into account using the Polarizable Continuum Model (PCM) with the integral equation formalism variant (IEFPCM) as a default Self-consistent Reaction Field (SCRF) method (Tomasi et al., 2005; Miertus et al., 1981). The IEFPCM model is considered to be a convenient one, because the second energy derivative is available for this model and its analytic form is also available. Our calculation was performed in the presence of a solvent (water molecule) by placing the PA or OD-PA solute in the cavity within the reaction field of the solvent. Since the dielectric constant of ice (85.5) is slightly higher than that of water (78.5), the vibrational frequencies reported here are not exactly those that pertain to ice but are close to these values.

In Table 5, we present the vibrational frequencies and intensities of PA and OD-PA in both the gas and ice phases. We show the band assignments and compare our results with the existing low resolution experimental results (Sivaraman et al., 2015; Nyquist, 1971). Vibrational detections of molecules in the interstellar medium may increase in importance with the impending launch of the James Webb Space Telescope (JWST) although the spectroscopic resolution may not be sufficient for rotational substructure in the gas.

We find that the most intense mode of PA in the gas phase appears at 1070.33 cm^{-1} , which corresponds to CO stretching with an integral absorbance coefficient of $1.70 \times 10^{-17} \text{ cm molecule}^{-1}$. This peak is shifted downward in the ice water phase by nearly 17 cm^{-1} and appears at 1053.89 cm^{-1} with an integral absorbance coefficient $2.46 \times 10^{-17} \text{ cm molecule}^{-1}$. Our frequencies can be compared with the experimental ice

Table 3: Peak abundances of PA, OD-PA and their related species with respect to H₂.

Species	Isothermal phase				Warm-up phase					
	gas phase		ice phase		gas phase			ice phase		
	Time (year)	Abundance	Time (year)	Abundance	Time (year)	T (K)	Abundance	Time (year)	T (K)	Abundance
PA	3.29×10^5	1.07×10^{-12}	7.40×10^5	5.03×10^{-10}	1.10×10^6	200.0	1.20×10^{-09}	1.01×10^6	32.2	7.09×10^{-11}
OD-PA	2.89×10^5	1.32×10^{-13}	5.66×10^5	1.33×10^{-11}	1.10×10^0	200.0	2.14×10^{-12}	1.02×10^6	47.3	7.23×10^{-12}
C ₃ H ₃	9.36×10^5	2.52×10^{-10}	1.85×10^5	4.32×10^{-13}	1.034×10^6	75.0	1.92×10^{-9}	1.022×10^6	50.9	3.25×10^{-14}
HC ₂ CHO	8.22×10^4	6.71×10^{-10}	2.17×10^5	2.60×10^{-10}	1.028×10^0	63.5	1.66×10^{-9}	1.01×10^6	29.2	2.05×10^{-9}
HC ₂ CH ₂ O	5.14×10^5	5.26×10^{-15}	1.85×10^5	9.43×10^{-18}	1.054×10^6	114.1	2.52×10^{-13}	1.01×10^6	29.2	7.23×10^{-17}

Table 4: Calculated line parameters for mm-wave transitions of Propenal, PA and OD-PA with ALMA

Species	ALMA Band	Frequency (GHz)	$J_{k_a' k_c'} - J_{k_a'' k_c''}$	E_{up} (K)	A_{ij}	Intensity (mK)
Propenal	Band 1	44.4975	$5_{05} - 4_{04}$	6.4	4.33×10^{-6}	287
Propenal	Band 2/Band 3	89.05935	$10_{46} - 9_{45}$ $10_{47} - 9_{46}$	56.44	3.06×10^{-5}	2320
Propenal	Band 3	115.80341	$13_{410} - 12_{49}$ $13_{49} - 12_{48}$	71.83	7.34×10^{-5}	3920
PA	Band 1	44.54410	$5_{05} - 4_{04}$	6.42	5.03×10^{-7}	8.18
PA	Band 2/Band 3	89.39184	$10_{65} - 9_{64}$ $10_{64} - 9_{63}$	72.01	2.74×10^{-6}	102
		89.39212	$10_{56} - 9_{55}$ $10_{55} - 9_{54}$	57.23	3.21×10^{-6}	102
PA	Band 3	116.23546	$13_{59} - 12_{58}$ $13_{58} - 12_{57}$	72.68	8.10×10^{-6}	160
		116.23586	$13_{86} - 12_{85}$ $13_{85} - 12_{84}$	125.04	5.97×10^{-6}	160
OD-PA	Band 1	44.88953	$5_{14} - 4_{13}$	7.68	4.93E-7	0.013
OD-PA	Band 2/Band 3	87.65146	$10_{55} - 9_{54}$	53.43	3.43×10^{-6}	0.112
OD-PA	Band 3	113.96386	$13_{59} - 12_{58}$	68.58	8.59×10^{-6}	0.206
		113.96429	$13_{58} - 12_{57}$			

Band 1= 31-45 GHz

Band 2= 67-90 GHz

Band 3= 84-116 GHz

phase value of 1030.7 cm^{-1} (Sivaraman et al., 2015) and the vapor phase value of 1051 cm^{-1} (Nyquist, 1971). Other strong modes of vibrations are the OH torsion, CCC bending, CH₂ wagging, CH stretching, and OH stretching. In the case of OD-PA, the CCO stretching mode is the most intense mode and appears at 1068.32 cm^{-1} in the gas phase and 1050.98 cm^{-1} in the ice phase with integral absorbance coefficients of 1.61×10^{-17} and $2.49 \times 10^{-17} \text{ cm molecule}^{-1}$ respectively.

Table 5 clearly shows the differences between spectroscopic parameters computed for propargyl alcohol between the two phases. These differences can be explained due to electrostatic effects, which are often much less important for species placed in a solvent such as water with high dielectric constant than they are in the gas phase but these changes will be significant if both the solvent and the molecule are polar.

The two sets of results for PA are in good agreement as regards frequencies with the existing experimental results, as shown above for the single case of the strong CO stretching. Differences between the results could be attributed to multiple reasons, one of which concerns the Gaussian 09 program, with which we are unable to consider the mixing of different modes under harmonic oscillator approximations. Another reason is that in our quantum chemical simulation of ice spectra, we considered a single propargyl alcohol molecule inside a spherical cavity and immersed it in a continuous medium with a dielectric constant, while in the experiment propargyl alcohol was deposited atop the ice, which could lead to the formation of clusters.

5. Conclusions

Earlier results suggest that PA could be treated as a precursor of benzene formation (Wilson et al., 2003). The interstellar identification of propenal, which is an isomer of PA, encouraged us to check the possibility of detecting PA and OD-PA in the ISM. Our quantum chemical calculations, combined with existing rotational transition frequencies for PA and OD-PA, allow us to achieve the following major results for this paper:

- A complete reaction network has been prepared for the formation and destruction of PA. Various formation routes are discussed and identified based on calculated exothermicities and endothermicities.
- The predicted abundances of PA and OD-PA in the gas and ice phases yield some information for both cold and warm interstellar sources on the possibility of observing this molecule in the ISM, especially in hot-core regions such as Sgr B2(N).
- A simple radiative transfer model has been employed to discuss the possibility of detecting PA in the ISM through millimeter-wave observations. The most likely environments for detection of PA are hot-core regions with a temperature above 100 K.
- The frequencies and intensities of vibrational transitions of PA and OD-PA both in the gas and in a mimetic for an ice environment are calculated and compared with existing low resolution experimental frequencies. The calculated intensities should be particularly useful.

Table 5: Vibrational frequencies and intensities of PA and OD-PA in the gas phase and in water ice at the MP2/aug-cc-pVTZ level of theory

Species	Peak positions (Gas phase) (cm ⁻¹)	Integral absorbance coefficient) (cm/molecule)	Peak positions (H ₂ O ice) (cm ⁻¹)	Integral absorbance coefficient (cm/molecule)	Band assignments	Experimental values (cm ⁻¹)
PA	186.09	1.48×10 ⁻¹⁸	192.71	1.09×10 ⁻¹⁸	CCC out of plane bending	240 ^a
	257.59	1.02×10 ⁻¹⁷	258.48	1.59×10 ⁻¹⁷	OH torsion	—
	319.40	9.89 ×10 ⁻¹⁸	330.49	1.64×10 ⁻¹⁷	CCC bending	305 ^a
	554.56	1.91×10 ⁻¹⁸	555.37	2.97×10 ⁻¹⁸	CCO bending	558.6 ^b 550 ^a
	640.33	7.43 ×10 ⁻¹⁸	647.20	1.08×10 ⁻¹⁷	CH bending	639 ^a
	665.86	6.09×10 ⁻¹⁸	672.76	8.99×10 ⁻¹⁸	CH out of plane bending	654 ^b 657 ^a
	922.65	4.37×10 ⁻¹⁸	922.89	5.97×10 ⁻¹⁸	C-C stretching	916.8 ^b 918 ^a
	1002.52	2.89×10 ⁻¹⁸	987.69	6.28×10 ⁻¹⁸	CH ₂ rocking	987.2 ^b 980 ^a
	1070.33	1.70×10 ⁻¹⁷	1053.89	2.46×10 ⁻¹⁷	C-O stretching	1030.7 ^b 1051 ^a
	1225.86	2.61×10 ⁻¹⁸	1224.44	3.85×10 ⁻¹⁸	CH ₂ twisting	1228 ^a
	1355.10	4.50×10 ⁻¹⁹	1371.30	9.84×10 ⁻¹⁹	CH/OH bending	—
	1417.76	8.47×10 ⁻¹⁸	1409.79	1.03×10 ⁻¹⁷	CH ₂ wagging	1362 ^b
	1517.33	2.70 ×10 ⁻¹⁹	1505.02	5.81×10 ⁻¹⁹	CH ₂ scissoring	1480 ^a
	2131.06	2.92×10 ⁻¹⁹	2125.63	4.23×10 ⁻¹⁹	CC stretching	2185 ^a
	3066.90	4.64×10 ⁻¹⁸	3084.99	4.92×10 ⁻¹⁸	CH ₂ symmetric stretching	2922 ^b 2930 ^a
	3145.17	8.51×10 ⁻¹⁹	3154.35	1.05×10 ⁻¹⁸	CH ₂ antisymmetric stretching	2940 ^a
	3483.14	9.39×10 ⁻¹⁸	3364.13	1.45×10 ⁻¹⁷	C-H stretching	3282 ^b 3322 ^a
	3831.50	6.97 ×10 ⁻¹⁸	3813.81	1.32×10 ⁻¹⁷	O-H stretching	—
OD-PA	164.70	3.97×10 ⁻¹⁸	173.05	5.27×10 ⁻¹⁸	OD torsion	—
	221.58	5.59×10 ⁻¹⁸	221.28	9.19×10 ⁻¹⁸	CCC out of plane bending	—
	307.17	3.08 ×10 ⁻¹⁸	313.58	5.01×10 ⁻¹⁸	CCC bending	—
	543.25	2.13×10 ⁻¹⁸	547.08	3.24×10 ⁻¹⁸	CCO bending	—
	640.32	7.35 ×10 ⁻¹⁸	647.20	1.08×10 ⁻¹⁷	CH bending	—
	665.39	6.12×10 ⁻¹⁸	672.72	9.03×10 ⁻¹⁸	CH out of plane bending	—
	885.79	5.89×10 ⁻¹⁸	852.99	8.03×10 ⁻¹⁸	OH bending	—
	961.44	2.40×10 ⁻¹⁸	944.47	3.55×10 ⁻¹⁸	CC stretching	—
	1068.32	1.61×10 ⁻¹⁷	1050.98	2.49×10 ⁻¹⁷	CCO stretching	—
	1086.19	5.05×10 ⁻¹⁹	1086.55	1.06×10 ⁻¹⁸	CH ₂ rocking	—
	1303.40	2.16×10 ⁻²⁰	1313.89	8.66×10 ⁻²⁰	CH ₂ twisting	—
	1396.85	4.39×10 ⁻¹⁸	1396.93	6.64×10 ⁻¹⁸	CH ₂ wagging	—
	1517.29	2.63 ×10 ⁻¹⁹	1504.99	5.71×10 ⁻¹⁹	CH ₂ scissoring	—
	2131.04	2.94×10 ⁻¹⁹	2125.63	4.25×10 ⁻¹⁹	CC stretching	—
	2789.51	4.50×10 ⁻¹⁸	2776.81	8.25×10 ⁻¹⁸	OD stretching	—
	3066.98	4.54×10 ⁻¹⁸	3085.06	4.83×10 ⁻¹⁸	CH ₂ symmetric stretching	—
	3145.44	7.29×10 ⁻¹⁹	3154.61	8.76×10 ⁻¹⁹	CH ₂ antisymmetric stretching	—
	3483.14	9.40 ×10 ⁻¹⁸	3464.13	1.46×10 ⁻¹⁷	CH stretching	—

^a Nyquist (1971) (vapor phase), ^b Sivaraman et al. (2015) (ice phase experiment)

6. Acknowledgments

PG, AD & SKC are grateful to DST (Grant No. SB/S2/HEP-021/2013) and ISRO Respond (Grant No. ISRO/RES/2/402/16-17) for financial support. LM thanks the ERC for a starting grant (3DICE, grant agreement 336474). E. H. wishes to acknowledge the support of the National Science Foundation for his astrochemistry program.

References

- Albertsson, T., Semenov, D.A., Vasyunin, A.I., Henning, T., & Herbst, E., 2013, *Astrophys. J. Supp. Ser.*, 207, 27. doi:10.1088/0067-0049/207/2/27
- Allamandola, L.J., Tielens, A.G.G.M., & Barker, J.R., 1985, *Astrophys. J.*, 290, L25-L28. doi:10.1086/184435
- Allen, M., & Robinson, G.W., 1977, *Astrophys. J.*, 212, 396-415. doi:10.1086/155059
- Becke, A.D., 1988, *Phys. Rev. A*, 38(6), 3098-3100. doi:10.1103/PhysRevA.38.3098
- Brenner, J.D., & Barker, J.R., 1992, *Astrophys. J.*, 388, L39-L43. doi:10.1086/186325
- Cami, J., Bernard-Salas, J., Peeters, E., & Malek, S.E., 2010, *Science*, 5996, 1180-1182. doi:10.1126/science.1192035
- Caselli, P., 2002, *Planet Space Sci.*, 50, 1133-1144. doi:10.1016/S0032-0633(02)00074-0
- Cazaux, S., Cobut, V., Marseille, M., Spaans, M., & Caselli, P., 2010, *Astron. Astrophys.*, 522, 74-87. doi: 10.1051/0004-6361/201014026
- Collings, M.S., Anderson, M.A., Chen, R., Dever, J.W., Viti, S., et al., 2004, *Mon. Not. R. Astron. Soc.*, 354, 1133-1140. doi:10.1111/j.1365-2966.2004.08272.x
- Cronin, J.R., & Chang, S., 1993, In *The Chemistry of Life's Origins*, ed. J. M. Greenberg, C. X. Mendoza-Gomez, V. Pirronello (Dordrecht: Kluwer), 209-258.
- Cuppen, H., & Herbst, E., 2007, *Astrophys. J.*, 668, 294-309. doi:10.1086/521014
- Das, A., Majumdar, L., Chakrabarti, S.K., & Sahu, D., 2015a, *New Astron.*, 35, 53-70. doi:10.1016/j.newast.2014.07.006
- Das, A., Majumdar, L., Sahu, D., Gorai, P., Sivaraman, B., & Chakrabarti, S.K., 2015b, *Astrophys. J.*, 808, 21-34. doi:10.1088/0004-637X/808/1/21
- Demyk, K., Bottinelli, S., Caux, E., Vastel, C., Ceccarelli, C., Kahane, C., & Castets, A., 2010, *Astron. Astrophys.*, 517, 17-22. doi:10.1051/0004-6361/200913830
- Devendra, M., & Arunan, E., 2013, *Chem. Phys. Chem.*, 14, 754-763. doi:10.1002/cphc.201200760
- Devendra, M., & Arunan, E., 2014 *J. Chem. Phys.*, 141, 164311. doi:10.1063/1.4898378
- Dong, H., Ding, Y., & Sun, C., 2005, *J. Chem. Phys.*, 122, 204321. doi:10.1063/1.1903945
- Evans, N. J., Dunham, M.M., Jorgensen, K.J., Enoch, M.L., et al. 2009, *Astrophys. J. Supp. Ser.*, 181, 321-350. doi:10.1088/0067-0049/181/2/321
- Eyring, H., 1935, *J. Chem. Phys.*, 3, 107-115. doi:10.1063/1.1749604
- Frisch, M.J., Trucks, G.W., Schlegel, H.B. et al., 2013, *GAUSSIAN 09*, (Wallingford CT: Gaussian Inc.)
- Garrod, R.T., 2013, *Astrophys. J.*, 765, 60-88. doi:10.1088/0004-637X/765/1/60
- Garrod, R.T., & Herbst, E., 2006, *Astron. Astrophys.*, 457, 927-936. doi: 10.1051/0004-6361/20065560
- Garrod, R.T., Weaver, S.L.W., Herbst, E., 2008, *Astrophys. J.*, 682, 283-302. doi: 10.1086/588035.
- Gredel, R., Lepp, S., Dalgarno, A., & Herbst, E., 1989, *Astrophys. J.*, 347, 289-293. doi:10.1086/168117
- Hasegawa, T., & Herbst, E., 1993, *Mon. Not. R. Astron. Soc.*, 261, 83-102. doi:10.1093/mnras/261.1.83
- Hasegawa, T., & Herbst, E., Leung, C.M., 1992, *Astrophys. J. Supp. Ser.*, 82, 167-195. doi:10.1086/191713
- Herbst, E., 2006, in *Springer Handbook of Atomic, Mol. & Opt. Phys.*, ed. G.W.F. Drake (New York: Springer), 561-574.
- Hirota, E., 1968, *J. Mol. Spectrosc.*, 26, 335-350. doi:10.1016/0022-2852(68)90069-6
- Hollis, J.M., Jewell, P.R., Lovas, F.J., Remijan, A., & Møllendal, H., 2004, *Astrophys. J.*, 610, L21-L24. doi: 10.1086/423200
- Jäger, C., Huisken, F., Mutschke H., Jansa, I.L. & Henning, T., 2009, *Astrophys. J.*, 696, 706-712. doi:10.1088/0004-637X/696/1/706
- Kwon, K., Nam, M., Youn, S., Joo, S., Lee, H., & Choi, J., 2006, *J. Chem. Phys.*, 124, 204320. doi:10.1063/1.2201996
- Lattalais, M., Bertin, M., Mokrane, H., Romanzin, C., Michaut, X., Jeseck, P., et al., 2011, *Astron. Astrophys.*, 532, A12. doi:10.1051/0004-6361/201016184
- Lee, C., Yang, W., & Parr, R.G., 1988, *Phys. Rev. B*, 58, 785-789. doi:10.1103/PhysRevB.37.785
- Lee, H., Nam, M., & Choi, J., 2006, *J. Chem. Phys.*, 124, 044311. doi:10.1063/1.2158989
- Leung, C.M., Herbst, E., Huebner, W.F., 1984, *Astrophys. J. Suppl. Ser.*, 56, 231-256. doi:10.1086/190982
- Millar, T., Bennett, A., & Herbst, E., 1989, *Astrophys. J.*, 340, 906-920. doi: 1989ApJ...340..906M
- Miertus, S., Scrocco, E., & Tomasi, J., 1981, *Chem. Phys.*, 55, 117-129. doi:10.1016/0301-0104(81)85090-2
- Noble, J.A., Dedonder, C., & Juvet, C., 2015, *Astron. Astrophys.*, 577, 79-89. doi:10.1051/0004-6361/201425493
- Nyquist, R.A., 1971, *Spectrochimica Acta*, 27A, 2513-2523. doi:10.1016/0584-8539(71)80148-4
- Pearson, J.C., & Drouin, B.J., 2005, *J. Mol. Spectrosc.*, 234, 149-156. doi:10.1016/j.jms.2005.08.013
- Peterson, K.A., & Dunning, T.H., 2002, *J. Chem. Phys.*, 117, 10548. doi:10.1063/1.1520138
- Petrie, S., 1995, *Astrophys. J.*, 454, L165-L168. doi:10.1086/309796
- Requena-Torres, M.A., Martin-Pintado, J., Martin, S., & Morris, M.R., 2008, *Astrophys. J.*, 672, 350-360. doi:10.1086/523627
- Roberts, H., & Millar, T.J., 2000, *Astron. Astrophys.*, 361, 388-398.
- Roberts, H., Herbst, E., & Millar, T.J., 2003, *Astrophys. J.* 591, L41-L44. doi:10.1086/376962
- Rodgers, S.D., & Millar, T.J., 1996, *Mon. Not. R. Astron. Soc.*, 280, 1046-1054. doi:10.1093/mnras/280.4.1046
- Salama, F., & Ehrenfreund, P., 2014, *IAUS*, 297, 364-369. doi:10.1017/S174392131301613X
- Sharath, N., Reddy, K.P.J., & Arunan, E., 2014, *J. Phys. Chem.*, 118, 5927-5938. doi:10.1021/jp505145j
- Sivaraman, B., Mukherjee, R., Subramanian, K.P., & Banerjee, S.B., 2015, *Astrophys. J.*, 798, 72-75. doi:10.1088/0004-637X/798/2/72
- Slagle, I.R., Gmuczyk, G.W., Batt, L., & Gutman, D., 1991, *Sym. (Int.) Combust.*, [Proc.] 23, 115-121.
- Su, T., & Chesnavich, W.J., 1982, *J. Chem. Phys.*, 76, 5183-5185. doi:10.1063/1.442828
- Tielens, A.G.G.M., & Allamandola, L.J., In: *Hollenbach, D.J., Thronson, H.A., 1987 (Eds.), Interstellar Processes*. Kluwer, Dordrecht, p. 397.
- Tomasi, J., Mennucci, B., & Cammi, R., 2005, *Chem. Rev.*, 105, 2999-3093. doi: 10.1021/cr9904009
- Upadhyaya, H.P., Kumar, A., Naik, P.D., Sapre, A.V., & Mittal, J.P., 2001, *Chem. Phys. Lett.*, 349, 279-285. doi:10.1016/S0009-2614(01)01218-0
- Walker, G.A. H., Bohlender, D. AS., Maier, J.P., & Campbell, E.K., 2015, *Astrophys. J.*, 815, L8-L12. doi:10.1088/2041-8205/812/1/L8
- Wakelam, V., Smith, I.W.M. Smith, & Herbst, E., et al., 2010, *Space Sci. Rev.*, 156, 1, 13-72. doi:10.1007/s11214-010-9712-5
- Wilson, E.H., Atreya, S.K., & Coustenis, A., 2003, *J. Geophys. Res.*, 108(E2), 5014. doi:10.1029/2002JE001896
- Woodall, J., Agundez, M., Markwick-Kemper, A.J., & Millar, T.J., 2007, *Astron. Astrophys. J.*, 466, 1197-1204. doi:10.1051/0004-6361/20064981
- Woon, D.E., & Herbst, E., 2009, *Astrophys. J. Supp. Ser.*, 185, 273-288. doi:10.1088/0067-0049/185/2/273
- Zhou, L., Zheng, W., & Kaiser, R.I., et al., 2010, *Astrophys. J.*, 718, 1243-1251. doi:10.1088/0004-637X/718/2/1243